Title

Biphasic Response of Protein Kinase A to Cyclic Adenosine Monophosphate Triggers Distinct Epithelial Phenotypes

Authors

João Pedro Fonseca[1], Elham Aslankoohi[1] and Hana El-Samad[1,2*]

[1] Department of Biochemistry and Biophysics, California Institute for Quantitative Biosciences, University of California, San Francisco, San Francisco, CA 94158, USA

[2] Chan Zuckerberg Biohub, San Francisco, CA 94158, USA

[*] To whom correspondence should be addressed: Hana.El-Samad@ucsf.edu

Abstract

Protein Kinase A (PKA) is an important cellular signaling hub whose activity has long been assumed to monotonically depend on the level of cyclic adenosine monophosphate (cAMP).

Using an optogenetic tool that can introduce precise amounts of cAMP in MDCKI cells, we demonstrate that PKA activity is instead characterized by a biphasic response, in which PKA activity increases and then decreases as a function of cAMP. We reveal that this behavior results from an elaborate integration by PKA of many cellular signals triggered by cAMP. In addition to the direct activation of PKA, cAMP also modulates the activity of p38 and ERK, which then converge on PKA to inhibit it. These interactions and their ensuing biphasic PKA profile have important physiological repercussions, triggering two distinct transcriptional programs elicited by

low and high cAMP doses. These transcriptional responses in turn influence the ability of MDCKI cells to proliferate and form acini. Our data, supported by computational analyses, synthesize a set of network interconnections involving PKA and other important signaling pathways into a model that demonstrates how cells can capitalize on signal integration to create a diverse set of responses to cAMP concentration and produce complex input-output relationships.

Introduction

Cyclic adenosine monophosphate (cAMP) is a secondary messenger that is an essential cellular currency in all kingdoms of life (1-3). In mammalian systems, cAMP is the major regulator of Protein Kinase A (PKA), an important cellular kinase that exerts regulation on a wide spectrum of cellular components, ranging from metabolic enzymes and cytoskeleton components to various transcription factors, such as the cAMP response element binding protein (CREB)(4-7). PKA is a holoenzyme composed of two regulatory subunits (PKAr) and two catalytic subunits (PKAc). Upon binding of cAMP to the PKAr, all subunits dissociate, allowing PKAc to phosphorylate and regulate its targets(8). Through this influence on PKA, cAMP controls a large swath of crucial cellular processes, such as proliferation, death and differentiation(3).

Because of its physiological importance, the level of cAMP is subject to intricate regulation on its production by adenylyl cyclases (AC) and degradation by phosphodiesterases (PDE)(3). It has been largely assumed that the activity of PKA correlates monotonically with the cAMP concentration.. However, this simple view of the functional relationship between cAMP and PKAhas recently been challenged. For example, it was demonstrated that the formation of memory in rodents shows a biphasic pattern that depends on cAMP level(9). When the hippocampus of mice was microinjected with low doses of cAMP analogs, they recalled their learnt behavior better than control mice. However, when treated with high doses of cAMP analogs,

mice were worse at retaining the learnt behavior. A similar physiological biphasic relationship was also noted between cAMP and the secretion rate of malpighi tubes of Drosophila(10). When these organs were stimulated with low levels of cAMP, produced either with cAMP analogs or with an optogenetically-controlled AC, they showed an increase in secretion rate. By contrast, when the dose of cAMP was large, tubes had a secretion rate that was lower than unstimulated organs. Furthermore, recent data have documented that serotonin (5-HT), a hormone known to increase cAMP intracellular concentration (11), promotes the biphasic activation and inactivation of PKA in mammary epithelial cells, and that these PKA patterns result in an increase and decrease of transepithelial electrical resistance (TEER), respectively(12). Intriguingly, the same work also demostrated that the stress related p38 MAPK (p38) is important for an overall inhibition of TEER, therefore suggesting that p38 and perhaps other MAPKs are involved in the regulation of PKA in a cAMP dependent fashion(12, 13). These data give hints of a complex relationship between PKA and cAMP in which multiple cellular pathways modulate the dependence of PKA on cAMP to generate a biphasic relationship that induce distinct phenotypes at different cAMP concentrations.

To systematically study this relationship, we employed the bacterial light-activated adenylyl cyclase bPAC (14). bPAC was isolated from the *Beggiatoa* bacterial genus, and is functional when expressed in other species such as yeast or mice(15, 16), showing low activity in the dark and rapid activation upon exposure to blue light to specifically elevate intracellular cAMP(14).

Unlike environmental and chemical inputs, bPAC specifically controls cAMP levels without interference or crosstalk with other cellular variables. It therefore provided us with a convenient tool to unambiguously probe the effects of cAMP dose on PKA activity and determine dose-dependent transcriptional response and physiological outcomes. We expressed bPAC in Madin-Darby Canine Kidney Type I (MDCKI) cells (17) where the cAMP-PKA pathway has been shown to regulate acini formation(18). Many renal epithelial phenotypes, such as control of cyst size (19),

podocyte differentiation(20), and fibrogenic programs in response to high glucose(21) are also controlled by the cAMP-PKA pathway. Therefore, understanding the effects of increasing cAMP concentrations in renal epithelial models, such as MDCK cells, is essential for understanding the biology of normal tissues as well as the pathological tissues in diseases such as diabetic glomerulopathy, nephrotic syndrome or polycystic kidney disease.

Our investigations using bPAC reveal that an increasing cAMP dose causally produces biphasic activity of PKA -- PKA activity increases and then decreases as a function of cAMP. ERK activity exhibits the same biphasic behavior as a function of cAMP dose but in the opposite direction, decreasing and then increasing as a function of cAMP. By contrast, p38 shows a monotonic dependence on cAMP. We show that the PKA inhibition at high cAMP dose is not generated by the known feedback loops regulating directly the level of cAMP, for example by regulation through increased PDE activity. Instead, we uncover that PKA activity is the result of a network of interactions involving cross-regulation with ERK and p38. We further demonstrate that the different behaviors of PKA at low versus high cAMP dose have important phenotypic consequences by eliciting two different cellular programs. We identify transcription factors that bind genes upregulated in both programs, as well as program-specific transcription factors, such as CREB that binds genes upregulated in low cAMP. Biological processes enriched in these two programs suggest that different cAMP doses differentially regulate many important phenotypes, such as proliferation and kidney morphogenesis. In particular, we show that concomitantly with changes in gene expression, the program elicited by a high dose of cAMP triggers increased proliferation and hampers the ability of the cell to form acini structures.

Together, these findings call for updating our understanding of PKA activity (at least in MDCK cells, and potentially in other systems) as a faithful monotonically dependent reporter of cAMP dose. Instead, we replace this notion with one in which PKA activity is finely tuned and modulated

by other cellular pathways. This modulation has large phenotypic consequences, eliciting phenotypes reminiscent of involvement of these cells in health and disease of the kidney.

Results

PKA and ERK show a biphasic response to bPAC-generated cAMP inputs in MDCK cells

To examine the effects of increasing cAMP inputs in MDCK cells, we expressed bPAC (22), a blue light responsive cyclase that we targeted to the cytoplasm (MDCKI + bPAC) (Figure 1A). To test the ability of bPAC to rapidly produce cAMP in this cell line, we measured cAMP levels by ELISA in the presence and absence of blue light. In the absence of light both MDCKI and MDCKI+bPAC had similarly low levels of cAMP (~1E-1 nM/ng protein, Figure 1B). After 20 minutes of continuous blue light exposure at maximum amplitude, only MDCKI+bPAC showed a large increase in intracellular cAMP (1318nM/ng protein, Figure 1B). To explore the range of intracellular cAMP concentrations that can be generated using bPAC, we further exposed MDCKI+bPAC cells to pulses of blue light of 30 second duration and varying duty cycles for 20 minutes. As expected, cAMP concentration increased with duty cycle (Figure 1C), reaching its maximum at continuous blue light exposure, demonstrating that bPAC can be used to generate a large range of precise cAMP levels spanning more than 3 orders of magnitude.

cAMP is a universal cellular messenger that acts upstream of PKA in all kingdoms of life (1). To determine the repercussions of increasing cAMP levels on PKA activity, we exposed MDCKI+bPAC cells to low (duty cycle = 1.7%) and high (duty cycle = 33%) bPAC inputs lasting 90 minutes and quantified PKA activity at different time points during light treatment by immunoblotting with antibodies that recognize the phosphorylated PKA target motif or phosphorylated cAMP Regulatory Element Binding Protein (CREB) (Supplementary Figure 1). Parental MDCKI cells did not show any changes in PKA activity for this regimen of light exposure

(Supplementary Figure 1). By contrast, PKA in MDCKI + bPAC cells was responsive to light activation. Specifically, PKA activity increased in cells exposed to low cAMP, reaching its maximum at 10 minutes (Supplementary Figure 1) and then declining to a new steady-state after that. Remarkably, however, PKA activity decreased when cells were exposed to high cAMP concentrations, with minimum activity reached at 5 minutes and maintained over the time course (Supplementary Figure 1). To quantify cAMP regimes that lead to an increase versus a decrease in PKA activity, we subjected MDCKI and MDCKI + bPAC cells to light inputs of different duty cycles, ranging from 0 to continuous exposure and quantified their PKA activity at 20 minutes, a time that was chosen because of the timescales of PKA activation and inactivation observed above. We identified that PKA activity increases with cAMP concentration and reaches its peak activity at ~1nM/mg protein (1.7% duty cycle). For cAMP concentrations above this value, PKA activity decreases, reaching values that are lower than its basal value for cAMP concentrations above 300nM/ng protein (Figure 1D and E). PKA activity, therefore, exhibits a markedly biphasic response to cAMP.

PKA activity is known to correlate negatively with mitogen activated kinase / extracellular signal-regulated kinase (ERK) pathway activity(23, 24). To further investigate the biphasic response elicited by cAMP, we measured ERK1/2 phosphorylation levels in MDCKI and MDCKI + bPAC cells subjected to the same light inputs as above. Remarkably, the ERK pathway showed a biphasic response as a function of cAMP, but one that was the opposite of PKA. In this response, doses of cAMP below 10nM/ng protein inhibited ERK1/2 below basal levels, with minimum activity appearing again around 1nM/ng cAMP protein (1.7% light duty cycle, Figure 1D and E, Supplementary Figure 1A). Above 10nM/ng cAMP inputs, ERK activation rose above its basal levels in the absence of stimulus. PKA has been implicated as a direct negative regulator of ERK activity and we hypothesized that ERK inhibition at low cAMP levels is the result of PKA activity(24). In agreement, when we treated cells subjected to no, low or high light inputs with H89

(a PKA inhibitor(25)), ERK activity increased above that of control cells (Supplementary Figure 2). Furthermore, the ERK activity of PKA-inhibited cells increased with duty cycle, suggesting that the ERK is activated by cAMP. Therefore, the biphasic behavior of ERK seems to be at least partially due to the competitive effects of direct activation by cAMP and inhibition by PKA.

Inhibition of PKA by high cAMP dose is independent of PDE activity and of the dissociation of PKA holoenzyme

To better conceptualize the molecular modalities by which cAMP can exert its physiological functions, we set to explore mechanisms of PKA regulation by cAMP and, in particular, of PKA inhibition by a high dose of cAMP, leading to its biphasic activity as a function of cAMP levels.

Previous investigations have described inactivation of PKA by two mechanisms involving feedback regulation that act primarily on cAMP. In the first mechanism, PKA activates PDEs that degrade cAMP thereby reducing PKA activity(26). In the second mechanism, PKA promotes the acidification of endosomes carrying AC-activating G protein–coupled receptors (GPCRs)(27). Since we were generating cAMP signals using an exogenous adenylyl cyclase, the second mechanism was less relevant. We therefore set out to test if PDE activity is required for PKA inhibition with high cAMP doses. We grew MDCKI + bPAC cells in the presence of DMSO or Rolipram to inhibit PDE activity for 1h, exposed them to varying doses of light for 20min, and then collected extracts from these cells and probed their PKA activity using immunoblotting (Supplementary Figure 3). As expected, inhibition of PDEs with Rolipram changed the input-output relationship from cAMP to PKA. PKA activity increased in the absence of light, and with cAMP inputs generated by duty cycles 0.3% and 1.7%, in cells exposed to Rolipram, when compared to DMSO (Figure 2A). Notably, however, for duty cycles larger than 1.7%, Rolipram treatment lead to the sharp inhibition of PKA activity, suggesting that cells reached the threshold

of cAMP concentration required for PKA inhibition with a smaller input of light due to the lack of cAMP degradation (Figure 2A). We therefore conclude that modulation of cAMP by PDE is not likely to be a major contributor to the biphasic relationship between PKA activity and cAMP.

Next, we tested whether this biphasic response is generated by molecular interactions of the PKA complex itself. One of the hallmarks of PKA activation by cAMP is the dissociation of its catalytic subunits from the regulatory subunits that are bound to A-kinase anchoring proteins (AKAPs)(5). PKA inhibition is also usually associated with the reassociation of the holoenzyme. We therefore explored the state of the PKA holoenzyme under different regimes of cAMP input to determine whether the association of the PKA subunits is preserved at high cAMP concentrations. In order to visualize PKA localization in MDCKI cells, we expressed the catalytic subunit of human PKA (PRKACA) fused to mRuby2. We quantified nuclear enrichment of PRKACA-mRuby2 as a proxy for its dissociation from PKA regulatory units and AKAPs. We first quantified PRKACA-mRuby2 nuclear enrichment in cells exposed to Forskolin (adenylyl cyclase activator) or H89 (PKA inhibitor). As expected, PKA activation by Forskolin lead to dissociation of PRKACA and increased its nuclear localization in both MDCKI and MDCKI + bPAC cells (Figure 2B). Due to the low basal activity of PKA, H89 treatment did not lead to a significant change in PRKACA localization, which remained mostly in the cytoplasm. Next, we investigated how bPAC-generated cAMP inputs changed the localization of PRKACA. To do so, we exposed MDCKI and MDCKI + bPAC cells to 20min of light with duty cycle 1.7% (low cAMP) or 33% (high cAMP), which increased or decreased PKA activity, respectively (Figure 1E). Light-induced low cAMP doses increased the nuclear fraction of PRKACA in bPAC-expressing cells to levels similar to those achieved by Forskolin treatment (Figure 2B). By contrast, the localization of PRKACA in the parental cell line did not change in either light conditions (Figure 2B). In MDCKI + bPAC cells exposed to the PKA-inhibiting high dose of cAMP, PRKACA nuclear localization increased to levels above those of low cAMP doses and those achieved following Forskolin treatment (Figure

194 2B). These data indicate that high levels of cAMP are not likely to inhibit PKA by directly increasing
195 the reassociation of the holoenzyme.

196 We therefore next explored whether the inhibition of PKA by high level of cAMP is a result of
197 network interactions, potentially involving MAPKs, that stem from cAMP and then converge on
198 PKA activity, subjecting it to competitive activating and inhibiting actions.

199

200 *p38 and ERK activation are required for inhibition of PKA by high cAMP doses*

201 Earlier work has shown that several pathways, including the p38 MAPK pathway, are activated
202 by cAMP in both PKA-dependent and independent manner(28). Additionally, it has been shown
203 that p38 can inhibit the PKA-dependent increase in TEER of epithelial cells(12) leading us to
204 hypothesize that the p38 MAPK pathway might be directly activated by cAMP in MDCKI cells, and
205 that it might converge onto PKA with inhibitory action (Figure 3A). To explore this possibility, we
206 measured p38 phosphorylation in MDCKI and MDCKI + bPAC cells in response to increasing
207 cAMP inputs, using immunoblotting. Light exposure did not increase p38 phosphorylation in
208 parental MDCKI cells (Figure 3B, C). By contrast, bPAC-expressing cells exposed to increasing
209 cAMP had a clear monotonic increase in phosphorylated p38 (Figure 3B, C).

210 To test whether p38 exerts inhibitory influence on PKA, we treated MDCKI + bPAC cells with the
211 p38 inhibitor SB202190, exposed them to varying doses of light for 20min and measured PKA
212 activity by immunoblotting. Inhibition of p38 increased PKA activity in MDCKI + bPAC cells across
213 all light treatments compared to cells treated with vehicle (DMSO) (Figure 3D, Supplementary
214 Figure 4), indicating that p38 indeed exerts an inhibitory influence on PKA. This inhibition,
215 however, was not uniform across all doses of light (that is, at different cAMP concentrations).
216 Instead, the difference in PKA activity between DMSO and SB202190-treated cells was larger at
217 0 duty cycle, suggesting that p38 was active and was important for setting the basal activity of

PKA. This difference then decreased between duty cycles of 0 and 3.3% and increased again with increasing duty cycles larger than 3.3% (Figure 3E).

While p38 inhibition changed the relationship between PKA and cAMP, therefore clearly implicating p38 in regulation of PKA activity, it wasn't able to completely abolish the decline of PKA activity at high cAMP levels. This implied that other inhibitory mechanisms are also at play. ERK signaling, whose activity negatively correlates with PKA (Figure 1E and F), is an obvious candidate for such regulation (Figure 3A). To investigate the role of ERK, we treated MDCKI + bPAC cells with U0216 (MEK inhibitor), then exposed cells to the same light doses as above and measured PKA activity by immunoblotting (Supplementary Figure 4). Cells with and without MEK inhibitor had the same relative PKA activity at light inputs below 3.3% duty cycle (Figure 3D), indicating that ERK activity had little influence on PKA at low levels of cAMP. However, U0126 treated cells had a reduced PKA inhibition at larger light inputs, suggesting that ERK activity was only effective in this regime. Taken together with the data demonstrating that ERK activity decreased for low cAMP and increased again for high cAMP (Figure 1F), we suspected that the most parsimonious model explaining the relationship between PKA and ERK is one in which they counteract each other in a double negative interaction (Figure 3A). Intuitively, in this model, ERK activity is a balance of activation by cAMP and inhibition by PKA. Low levels of cAMP cause large PKA activity, whose inhibitory effect dominates causing ERK activity to decrease (Supplementary Figure 2). At a certain threshold of cAMP though, the balance of power is flipped and ERK activity starts increasing, therefore subjecting PKA to inhibition at high cAMP doses (Figure 3E).

This reasoning does not take into account other interactions such as those of p38. We next explored whether the interactions between cAMP, PKA, ERK and p38, which were explored pairwise above, are able to produce the molecular phenotypes in the various experiments when considered together as an integrated system. To do so, we built a phenomenological mathematical model that captures these interactions in the cAMP-PKA signaling network. The

input to this model is cAMP (different amounts produced by bPAC) and the output is PKA activity (as a surrogate for the phosphorylation of its targets). In this model, cAMP activates PKA, p38 and ERK with different kinetics, and ERK and p38 inhibit PKA activity therefore mediating an incoherent feedforward interaction from cAMP onto PKA (Figure 3A, see methods and Supplementary Information). To potentially account for the biphasic response of ERK and the pattern of its inhibition data, the model also assumes that PKA inhibits ERK activation. These interactions were modeled phenomenologically using enzymatic Hill functions in order to allow for the possibility that the interactions are not direct, but instead can have multiple intermediate steps. This functional form also allows for cooperativity and saturation in the substrate. In this form, the model was easily able to reproduce all the data from bPAC as well as kinase inhibition experiments. However, several structural features of the model, as well as choice of its parameters were essential for this.

With regard to the topology of the model, the inhibition of ERK by PKA and the dependence of both kinases on cAMP for their activation were vital for the biphasic behavior of ERK (Figure 3H) as a function of cAMP in DMSO-treated cells. While ERK inhibition of PKA was not required by the model to recapitulate the biphasic response of PKA to cAMP (as illustrated by the reduction in PKA activity at high doses of light in the presence of U0126,Figure 3F), this inhibition was essential to induce a reduction in PKA activity in the absence of p38 activity (Figure 3F). In other words, if ERK inhibition of PKA did not exist, PKA activity could never decrease when p38 is inhibited because no negative influences on PKA would exist. Second, the monotonic rise in p38 activity with increasing duty cycles (Figure 3I) indicated that no inhibition of p38 by PKA was needed, an insight further corroborated by the ability of the model to fully reproduce the data without any feedback from p38 onto PKA (Figure 3F). However, a basal activity of p38 in the absence of the cAMP input was required in order to reproduce the basal increase in PKA activity upon inhibition of p38 by SB202190 (Figure 3F and G).

In terms of parameter constraints, to fully represent the phenotype of p38 inhibition, the model required larger levels of cAMP in order to activate p38 and hence to trigger its negative effect on PKA, giving PKA activity the opportunity to increase at low cAMP levels (Figure 3F and J). This was achieved by a larger K_m for the activation of p38 by cAMP (Km_{p38}) than that of PKA activation by cAMP (Km_{PKA}) (~27x larger in simulations, Supplementary Information, Supplemental Figure 5 A, B). When the K_m's of PKA and p38 were similar, the model achieved the activation of PKA by having a smaller Hill coefficient for the PKA activation (n_{PKA}) than p38 (n_{p38}) (Supplementary Figure 5 A, B and C). A different scenario in which Km_{p38} and Km_{PKA} were similar but the K_m of PKA inhibition by p38 (KmI_{p38}) is large should be formally able to produce the same effect. However, such a parameter regime produces PKA activity that is the same in the absence of cAMP between SB202190-treated cells and DMSO treated cells, which is contradictory with our data (Figure3F and J, Supplemental Figure 5).

Additionally, to reproduce the effects of ERK inhibition, the model required a larger $K_{m\ ERK}$ (K_m for the activation of ERK by cAMP) than K_{mPKA} (~32x larger, Supplementary Information, Supplemental Figure 5A, B) or a smaller n_{PKA} than n_{ERK} (Supplementary figure 5 A, B and C), and a high Hill coefficient for the ERK inhibition of PKA (n_{ERK} = 5.37, Supplementary Information, Supplemental Figure 5A and E). These parameters were necessary to reproduce the small effect of ERK inhibition on PKA activity for small cAMP inputs (Figure 3F and G) and its strong effect at high cAMP inputs. Intuitively, at low cAMP concentrations, PKA inhibition of ERK dominates and hence ERK plays a small role in modulating PKA activity (Figure 3J and K). However, as cAMP concentration increases and ERK passes a predicted sharp threshold where its activity starts increasing again (representing an inflection point in the ERK activity, Figure 1E), it starts exerting a negative effect on PKA (Figures 3J and K). This is the regime where inhibition of ERK has a notable effect as indicated by the data.

Finally, the model predicted that the inhibitory effect of p38 on PKA should increase noticeably only after cAMP inputs larger than Km_{p38} (duty cycle 6.7 and larger) and that it should reach saturation for duty cycle 100% (Figure 3L). The saturation of this inhibitory effect was essential for reproducing the quantitative pattern of PKA inhibition in the presence of U0126, where the rate of inhibition of PKA seemed to decrease at high duty cycles (from 33% to 100%, Figure 3F and G). Since in this experiment, only p38 is present as an inhibitory influence on PKA, and since its level continues to increase at these high duty cycles, the fact that PKA activity assumes similar values for different duty cycles while cAMP increases indicates that the influence of p38 on PKA has to reach a saturation. This saturation effect should also be present in cells treated with DMSO, which was absent in the experimental data (Figure 3Fand G), suggesting that additional interactions between the MAPKs that become important at high cAMP levels might also be present beyond the parsimonious model we have used.

Taken together, our data and computational modeling suggest that p38 activation modulates the activity of PKA through a cAMP-driven incoherent feedforward loop that plays an important role at all cAMP concentrations and that ERK engages in a double-negative feedback interaction whose importance seems to manifest at higher cAMP concentration. These interactions are integrated to produce a biphasic program of PKA activity for different cAMP concentrations. Given that PKA is a master regulator of cell physiology, we next turned to investigating whether this biphasic program has biological repercussions.

bPAC-generated cAMP inputs elicit differential transcriptional responses

PKA and ERK are known to target and modulate the activity of a wide array of transcription factors(6, 7). We therefore postulated that the ability of bPAC-generated cAMP to induce their biphasic response might have profound and distinct effects on the cellular transcriptome. To test

316 this hypothesis, we carried out mRNA sequencing of MDCKI and MDCKI+bPAC cells under no,
317 low, or high cAMP inputs (0%, 1.7% and 33% blue light duty cycle) for 2 hours.

318 In order to identify the effect of bPAC expression on cellular function in the absence of light, we
319 mined our dataset for genes that were differentially expressed in MDCKI + bPAC with no light
320 versus MDCKI parental cells (duty cycle = 0%). Additionally, we measured the effects of blue light
321 exposure on the MDCKI transcriptome by identifying genes that were differentially expressed in
322 MDCKI parental cells exposed to low or high light inputs (1.7% or 33%) versus no light input (0%).
323 We used DEseq2(29) to quantify Fold Change (FC) between conditions Using a threshold for fold
324 change in expression larger than 1.5 and an adjusted p-value smaller than 0.05 ($|FC|>1.5$, $p<0.05$,
325 see methods for justification of this choice), we identified 371 genes that were differentially
326 expressed due to bPAC expression and in the absence of light (Supplementary Figure 6).These
327 genes were enriched in Gene ontology(30) (GO) terms related to cellular adhesion and mitosis.
328 Reassuringly, these genes were not correlated with cAMP induced expression changes (see
329 below, Supplementary Figure 6). We also identified 434 genes that were differentially regulated
330 due to light exposure even in parental cell lines. These genes were removed from subsequent
331 analyses.

332 Our aim was to capture all genes that were differentially expressed in response to light-induced
333 cAMP inputs, and then classify them according to their patterns of cAMP dependence (monotonic
334 or biphasic dependence on cAMP). Using the same thresholds as above ($|FC|>1.5$, $p<0.05$), we
335 identified 3471 genes that are differentially expressed in response to one or both cAMP inputs,
336 as well as genes that are differentially expressed between cAMP doses (Figure 4A,
337 Supplementary table 1). We used hierarchical clustering to group them according to their patterns.
338 We identified 8 clusters that were further combined in 4 qualitatively different classes. Genes in
339 clusters 1 and 2 were strongly repressed in low cAMP and weakly repressed or activated in high
340 cAMP, hence showing correlation with ERK activity. On the other hand, genes in clusters 3 and

4 were strongly activated in low cAMP and weakly activated or repressed in high cAMP dose, therefore correlating with biphasic PKA activity. Finally, genes in clusters 5 and 6 were monotonically activated by cAMP while genes in clusters 7 and 8 were monotonically repressed by cAMP (Figure 4A and B). We confirmed the RNA sequencing results for four cAMP regulated genes with qPCR experiments on independent RNA samples (Supplementary Figure 7).

To distill the various transcriptional programs corresponding to the different classes, we performed Enrichr analysis(31) on genes from each class, focusing on transcription factors and kinases that regulate these genes and GO enrichment analysis to identify biological processes in which they are involved. Genes whose expression increased (clusters 5 and 6) or decreased (clusters 7 and 8) monotonically with cAMP concentration showed enrichment for the binding of specific transcription factors, such as NELFA or ELKF (Supplementary Figure 8), and regulation by kinases, such as SYK and AKT (Supplementary Figure 8). These genes were also enriched for GO terms related to chromatin remodeling, protein kinase A signaling, regulation of epithelium morphogenesis and DNA repair (Supplementary Figure 9). While the promotors of the genes in all clusters were enriched for the cAMP responsive element modulator (CREM) protein binding, suggesting a common dependency on cAMP, we decided to focus our thorough analyses on the clusters of genes that have a biphasic behavior, therefore reflecting the PKA or the ERK pattern, in order to identify the distinct genetic programs encoded by low and high cAMP doses (clusters 1-2 and 3-4). We expected that genes whose expression correlate with ERK activity (clusters 1 and 2) could be controlled by transcriptional regulators that are activated by ERK, or by transcriptional regulators that are inactivated in the absence of PKA activity. We found examples that matched the two hypotheses. First, this set of genes was specifically enriched for Vitamin D Receptor (VDR) and GA binding protein (GABP) binding (adjusted p-values $1.6x10^{-14}$ and $1.0x10^{-10}$, Supplementary Figure 8), which have been shown to have activity that is modulated by ERK(32, 33). We also found enrichment for genes that are up-regulated upon CREB1 depletion

(adjusted p-value $2.2x10^{-13}$, Supplementary Figure 8), whose activity is PKA-dependent(34). Interestingly, we also found that the set of genes whose expression correlates with ERK activity (clusters 1 and 2) was enriched for genes that are upregulated in a protein kinase B (AKT1) knockout and downregulated in the presence of an AKT1 active mutant (adjusted p-values $2.1x10^{-5}$ and $1.8x10^{-9}$, Supplementary Figure 8). These data suggest that AKT1 might also be differentially regulated by cAMP dose and that its activity should correlate negatively with ERK activity. To confirm these predictions, we measured phosphorylation level of AKT in parental MDCKI and MDCKI + bPAC cells exposed to low or high cAMP inputs. While there were no changes in AKT activity when the parental cell line was exposed to light, bPAC-carrying cells increased phospho-AKT levels with low doses of cAMP and quenched them at high cAMP doses (Supplementary Figure 10), again showing a biphasic response.

Next, we extended our analysis to the gene set whose expression correlated with PKA activity (clusters 3 and 4), again hypothesizing that their pattern of expression either followed PKA activity (they are activated by PKA-responsive transcription factors), or followed the absence of ERK regulated activators (they are repressed by ERK-responsive transcriptional regulators). These clusters were enriched in genes that are known targets of CREB1 and the histone demethylase KDM5B (adjusted p-values $1.0x10^{-14}$ and $1.3x10^{-13}$, Supplementary Figure 8), an effect that is likely mediated by PKA-driven regulation of chromatin remodelers and its activation of CREB1 transcription factor. In addition, we found a clear enrichment for genes that are known to be upregulated following knockout of the transcription factor jun-B (JUNB, adjusted p-value $1.2x10^{-13}$, Supplementary Figure 8), which is known to be activated by ERK as an immediate-early gene(35). As a result, ERK is likely to exert a repressive effect on these genes, and their pattern (e.g. activation at low cAMP) is therefore a result of differential alleviation of this repression as a function of cAMP.

Finally, we performed GO enrichment analysis for the 2 gene classes (Supplementary Figure 9). Genes belonging to clusters 1 and 2 (ERK correlated) were enriched in GO terms that encompassed desmosome organization, stress activated MAPK cascade and positive regulation of respiratory burst (Figure 4C, Supplementary Figure 9). By contrast, genes in clusters 3 and 4 (PKA correlated) had strong enrichment for terms related to chromatin remodeling, kidney morphogenesis and negative regulation of proliferation (Figure 4D, Supplementary Figure 9).

Together these findings suggest that the biphasic signaling responses of PKA and MAPK activity in MDCKI cells to cAMP dose propagates to gene expression, therefore potentially programming a large array of cellular phenotypes, ranging from proliferation, cell-cell and cell-extracellular matrix interactions, metabolism, and kidney morphogenesis.

Cellular proliferation is positively influenced by high cAMP inputs

Many genes in clusters 3 and 4 were associated with negative control of cellular proliferation, and these were repressed in the presence of high cAMP levels. This suggested that at a high cAMP dose, repression of these genes positions MDCKI cells to a state similar to cells transiting to a mesenchymal state(36) or in elongating regions of epithelial tubes, which have weaker cell-cell interactions and higher rates of proliferation(37, 38). To test this possibility, we exposed parental MDCKI and MDCKI + bPAC cells to no, low or high cAMP doses (duty cycle of 0, 1.7 and 33%) for 2 hours and measured their mitotic fraction by histone H3S10 phosphorylation after 14h. As expected, there were no significant changes in the mitotic fraction of MDCKI parental cells exposed to light. Yet, MDCKI + bPAC cells stimulated with a high cAMP dose had a marked ~5-fold increase in their proliferation rate when compared to unstimulated cells (Figure 5A). Cells exposed to the low cAMP input did not have a statistically significant change in the mitotic rate (~1.5-fold reduction in comparison to cells exposed to 0% duty cycle) (Figure 5A), indicating that

414 only high cAMP treatment can significantly change the proliferation rate of MDCKI cells. These
415 data support the notion that different doses of the same secondary messenger (cAMP), which
416 result in different signaling and transcriptional patterns, can be decoded by cells to regulate
417 proliferation in a differential way.

418

419 *Formation of MDCKI acini is differentially controlled by cAMP dose*

420 We noted that kidney developmental genes and cell adhesion genes belonged to the class of
421 genes that correlate with PKA activity (clusters 3 and 4, Figure 4A and B). In addition, both PKA
422 and ERK signaling pathways have been shown to regulate different stages of kidney
423 development(19, 39, 39). Therefore, we predicted that different cAMP doses, through their
424 biphasic influence on PKA and ERK, might influence the formation and maintenance of kidney
425 structures differently. To examine this effect, we focused on acinar development of MDCKI cells.
426 MDCK acinus formation is a well-studied model of kidney epithelial structure and function(40, 41).
427 Correct formation and maintenance of MDCKI acini relies on the precise coordination of events
428 that incorporate cell interactions with basement membrane, cell polarization, formation of tight
429 junctions and dependence on an abundance of extracellular signals(18).

430 It is known that PKA activity and ERK inhibition is required for the rapid formation of acini(23).
431 Therefore, we hypothesized that low cAMP doses and accompanying high PKA activity leads to
432 the development of acini of normal size, while high doses of cAMP and associated ERK activation
433 lead to increased cellular mobility and concomitant incorrect acinar development. To test this
434 hypothesis, we quantified acinar size in MDCKI and MDCKI+bPAC cells grown in collagen gels
435 exposed to no, low or high cAMP inputs for 10 days. MDCKI cells exposed to all light conditions
436 showed no significant change in the area of their acini (Figure 5B), demonstrating that the effects
437 of light are negligible on acini formation and maintenance. By contrast, cAMP dose had a striking

effect on the area of bPAC-expressing acini (Figure 5B). Specifically, we identified that low and high cAMP inputs had a significant effect on the distribution of acini area, in which the low dose of cAMP increased the area of acini (median increase of 1.6-fold when compared to no cAMP), and acini exposed to high doses of cAMP showed a reduction in their area (median reduction of 1.7-fold when compared to no cAMP) (Figure 5B). These data illustrate that tight control of intracellular cAMP concentration and signaling activity is vital for the correct formation of multicellular structures, and that MDCKI cells can use cAMP concentration and its paradoxical effect on downstream pathways to generate an array of multicellular epithelial phenotypes.

Discussion

In this work, we used a combination of precise optogenetic stimulation to control cAMP levels in living cells, with various cell biological readouts of its impact, to investigate the relationship between cAMP dose and the PKA signaling pathway. We uncovered that PKA and ERK activity is biphasic as a function of cAMP, with PKA activity increasing and then decreasing as a function of cAMP and ERK activity showing the opposite behavior. To understand the repercussions of these different dependencies, we used mRNA sequencing under two cAMP regimes (low and high) to demonstrate that they indeed correspond to two different molecular programs and physiological outcomes. Molecularly, we explored the intricate roles of p38 and the ERK pathways in producing the biphasic PKA phenotype and presented a data-supported model in which a poorly studied interaction between PKA and MAPKs inhibits PKA signaling pathway in a cAMP-dependent way. As a result, PKA is under positive and negative influences from cAMP, with the negative influence mediated by MAPKs. The interaction of these two modes of regulation, and their relative strength, induces a non-monotonic dependence of PKA on cAMP in the MDCKI cells we study here.

462 The biphasic response of PKA to cAMP has been previously observed in malpighi tubes of
463 flies(10), hypothalamus of mice(9), and human mammary cells(12) stimulated with small
464 molecules. However, the non-monotonic behaviors reported in most of these earlier works
465 resulted from chemical inputs that perturbed many cellular nodes, other than cAMP. Our use of
466 bPAC allowed us to circumvent this pleiotropy and uncouple feedback regulation on cAMP
467 production from PKA activity. As a result, we could unambiguously link PKA activity solely to the
468 amount of cAMP produced by bPAC and hence causally link cAMP concentration to the biphasic
469 response of the PKA pathway. Additionally, this precise cAMP input afforded by bPAC enabled
470 us to causally establish additional downstream targets of cAMP, including ERK, AKT and p38.

471 The biphasic nature of PKA and ERK responses to cAMP is implemented both by the incoherent
472 feedforward loop (IFFL) motif from cAMP to PKA through the activities of p38 and ERK, and by
473 the mutual inhibition of PKA and ERK. It is unknown how p38 and ERK produce their negative
474 effect on PKA signaling. Our transcriptional dataset indicated that DUSPs are upregulated upon
475 high cAMP doses, suggesting that they might mediate some of this interaction. However, further
476 studies will be necessary to discover if their phosphatase activity is altered, if PKA and its targets
477 are also targeted by these DUSPs, or if additional mechanisms are involved. Furthermore, it is
478 unclear how ERK and p38 are activated by cAMP. While previous studies have shown activation
479 of MAPKs by cAMP through the activity of PKA(42), our results suggest that, in MDCKI cells,
480 additional cAMP-dependent mechanisms are involved. Previous results suggest that EPAC, PKA
481 regulatory subunits and β-arrestins can initiate the activation of MAPK signaling pathways(28, 43-
482 45). It is therefore possible that one or more of these mechanisms are responsible for the
483 activation of MAPKs at high cAMP doses.

484 Irrespective of the precise molecular mechanisms underlying cAMP effect on MAPKs and the
485 effect of MAPKs on PKA, the presence of at least two IFFL structures in the system is at the heart
486 of its biphasic behavior. An IFFL is a circuit motif that that is usually assumed to respond to a step

input with a transient response that then adapts close to its unstimulated state (46). However, a less studied operational regime of IFFL is one in which they can give rise to dose-dependent biphasic responses(47, 48), such as the ones shown here. We explored these regimes in the context of the cAMP-PKA computational model and identified its specific parameter requirements. It is interesting to think that in other cell types, or even in disease states, changes in parameter values or network topology can give origin to radically different signaling responses out of the same molecular players. For example, if PKA is unable to inhibit ERK, ERK activity would increase monotonically with cAMP concentration. As a result, the signaling state of cells would be that of active PKA and ERK, instead of active PKA and inhibited ERK, at low cAMP concentration. It is far from clear what new functionalities or pathologies might ensue from these different signaling states. This is particularly important in light of the fact that the capacity of cAMP to coordinate the activity of important signaling pathways in MDCKI cells led to important changes in the expression of many genes. Remarkably, several of those genes that were cAMP responsive followed either a PKA or an ERK pattern, and correspondingly implemented two different programs. In the high cAMP program (repressed PKA and activated ERK) the proliferation rate of cells was increased and their ability to form acini reduced. By contrast, at a lower cAMP dose, proliferation rate was smaller than at a high cAMP dose and the size of acini was larger, in accordance with the previously described effects of PKA on acinar morphogenesis(23). Interestingly, in Polycystic Kidney disease (PKD) cells, PKA is thought to activate MAPK and that activity of both pathways is required for the measured increase in proliferation rate and acinus size(19). It is unclear if cells are producing abnormal cAMP doses or if the decoding of cAMP dose is deficient. While therapies for PKD have focused on reducing cAMP levels(49), if the network topology present in MDCKI cells is conserved in PKD cells, an alternative approach would be to increase cAMP, or directly activate p38, to inhibit PKA activity and reduce cystogenesis. Finally, while the particular interactions in the cAMP-PKA-MAPK network we uncover here might be specific to epithelial cells, it is fascinating to think about how these links might be modulated, to shift the quantitative

relationship between cAMP and PKA in different cell types. For example, a quantitative change in the inhibition of PKA by p38 or ERK might shift where PKA activity reaches its peak as a function of cAMP. A different change, balancing the timescale of the inhibiting and activating links on PKA, might abolish the biphasic relationship altogether. One can also imagine that some cell types might modulate these links dynamically, using inputs other than cAMP to impinge on the relationship of p38 and ERK on PKA, weakening or strengthening it based on the particular circumstances encoded in these inputs.

Methods and Materials

Cell culture

MDCKI cell line was a kind gift from Pavel Nedvestky. No mycoplasma contamination was found. MDCKI + bPAC cells were generated by infecting MDCKI cells with pLenti-PGK-bPAC::NES (Addgene #130267). PKAc expressing cells were obtained by transfecting MDCKI and MDCKI + bPAC cells with pPB-CAG-PRKACA::mRuby2 (Addgene #130268). Cells were maintained in MEM (Gibco #11095072) supplemented with 10% Fetal Calf Serum (VWR #89510-184) and 1X Anti-Anti (Gibco #15240062), and kept at 37 °C in a humidified incubator with 5% CO2.

Antibodies and reagents

To probe signaling activity we used the following antibodies: anti-Phospho-PKA Substrate (RRXS*/T*) (100G7E) Rabbit mAb (Cell signaling technology #9624S, 1:2000), anti-Phospho-CREB (Ser133) (87G3) Rabbit mAb (Cell signaling technology # 9198S, 1:2000), anti-p44/42 MAPK (Erk1/2) (L34F12) Mouse mAb (Cell signaling technology ##4696, 1:2000), anti-

Phospho-p38 MAPK (Thr180/Tyr182) (D3F9) XP® Rabbit mAb (Cell signaling technology #4511, 1:2000), anti-αTubulin Antibody (DM1A) (Santa Cruz biotechnology #sc-32293, 1:2000), anti-Phospho-Akt (Thr308) (D25E6) XP Rabbit mAb (Cell signaling technology #13038S, 1:2000), anti-Phospho-Histone H3 (Ser10) Antibody (Cell signaling technology #9701, 1:500), IRDye 800CW Donkey anti-Rabbit (LI-COR #925-32213, 1:10000), IRDye 680RD Donkey anti-Mouse (LI-COR #925-68072, 1:10000) and Anti-rabbit IgG (H+L), F(ab')2 Fragment (Alexa Fluor® 488 Conjugate) (Cell Signaling Technology #4412, 1:1000).

The following small molecules were used: SB202190 (Selleck Chemicals, #S1077, 10μM), U0126 (MedChem Express #HY-12031, 10μM), rolipram ((R)-(-)-Rolipram, Tocris #1349, 100μM), H89 (H 89 dihydrochloride, Tocris #2910, 10μM) and Forskolin (Tocris # 1099/10, 50μM).

Quantification of cAMP

1x10^6 cells were seeded in wells of 6-well plates (FALCON # 353046) in MEM without phenol red (Gibco # 51200038) supplemented with 0.5% Fetal Calf Serum (VWR #89510-184). After 16h, cells were exposed to no light or blue light (2.2 $mW.cm^{-2}$) with different duty cycles for 20min. After light exposure cells were transferred to ice and cAMP concentration was determined using the cAMP ELISA Kit (Cell biolabs #STA-501), following the manufacturer's instructions. To determine protein concentration, ELISA samples were assayed using the Pierce BCA Protein Assay Kit (Thermo Scientific Pierce #23227), following the manufacturer's instructions. Measurements for cAMP ELISA and BCA Protein Assay kits were performed in a FlexStation 3 Multi-Mode Microplate Reader (Molecular Devices). The cAMP dose response to light was fit to a hyperbolic equation and confidence intervals were extracted by bootstrapping in a custom Python Script available on GitHub (https://github.com/jpfon/cAMP).

560

561 *Quantitative western blot*

562 1x10^6 cells were seeded in wells of 6-well plates (FALCON # 353046) in MEM without phenol
563 red (Gibco # 51200038) supplemented with 0.5% Fetal Calf Serum (VWR #89510-184). After
564 16h, cells were treated with inhibitors or vehicle (DMSO, SIGMA life science #D2650) for 1h.
565 Cells were then exposed to no light or blue light (2.2 $mW.cm^{-2}$) with different duty cycles for
566 20min. Cells were lysed in cold M-PER (Thermo Scientific Pierce #PI78501) supplemented with
567 protease (Thermo Scientific Pierce #PIA32953) and phosphatase (Thermo Scientific Pierce #PI-
568 88667) inhibitors for 20min. Proteins were separated in 7.5% Mini-PROTEAN® TGX™ Precast
569 Protein Gels (Biorad), probed with primary antibodies diluted in blocking buffer (Rockland
570 Immunochemical #MB-070) for 16h and with secondary antibodies diluted in blocking buffer for
571 2h. Proteins were detected by fluorescence in a Odyssey CLx (LI-COR). Phospho-PKA
572 Substrate quantification was performed for proteins above 75KDa. Tubulin was used as a
573 loading control. Quantification was done using ImageJ (NIH) and a custom Python Script
574 available on GitHub (https://github.com/jpfon/cAMP).

575

576 *RNA library preparation and sequencing*

577 1x10^6 cells were seeded in wells of 6-well plates (FALCON # 353046) in MEM without phenol
578 red (Gibco # 51200038) supplemented with 0.5% Fetal Calf Serum (VWR #89510-184). After
579 16h, cells were exposed to no light or blue light (2.2 $mW.cm^{-2}$) with different duty cycles for 2h.
580 After light exposure cells were transferred to ice and total RNA was isolated using SPLIT RNA
581 Extraction Kit (Lexogen # 008.48), following the manufacturer's instructions. RNA quality was
582 assessed using RNA 6000 Nano chips (Agilent # 5067-1512) in a Bioanalyzer 2100 (Agilent).
583 RNA libraries for Illumina sequencing were prepared from 2ug of total RNA, using the QuantSeq

3' mRNA-Seq Library Prep Kit FWD for Illumina (Lexogen # 015.96). Library quality was assessed using High Sensitivity DNA kit (Agilent # 5067-4626) in a Bioanalyzer 2100 (Agilent). Sequencing was performed at the Center for Advanced Technology (UCSF), in a HiSeq 4000 (Illumina). One lane was used to generate 50bp single reads. Sequencing data is available GEO (GSE134650)

RNA sequencing analysis

Low quality reads and reads containing adapters were removed from raw data. Gene counts were generated using the standard workflow of Bluebee NGS Genomics Analysis Software (QuantSeq-FWD) for the dog genome (https://platform.bluebee.com). Differentially expressed (DE) genes were identified using the DESeq2 R package(29), with |logFC| >1.5 adjp >0.05, in order to reduce the false discovery rate and genes whose expression change was small. Clustering of DE genes was performed using a custom R script available on GitHub (https://github.com/jpfon/cAMP). Gene Ontology term enrichment for genes in each cluster was performed using DAVID(30) and displayed in a 2D scatterplot based on the semantic similarity (Revigo(50)). Transcription factor and kinase regulation enrichment analysis was performed using Enrichr (31).

Quantitative RT-PCR

Total RNA was prepared as described in the RNA library preparation section. First strand synthesis was performed on 5ug of RNA using Superscript II (Invitrogen #18064-014) and following the manufacturer's instructions. qPCR was performed in a CFX connect (Bio Rad), using the PerfeCTa SYBR® Green FastMix (Quantabio #95072) and following the

manufacturer's instructions for Fast 2-Step Cycling. GUSB expression was used as normalization factor. Primers used are shown in Supplementary Table 2.

Quantification of mitotic fraction

4x10^4 cells were seeded in wells of 8-well slides (Ibidi # 80826) in MEM without phenol red (Gibco # 51200038) supplemented with 2% Fetal Calf Serum (VWR #89510-184). After 16h, cells were exposed to no light or blue light (2.2 mW/cm^2) with different duty cycles for 2h. After 14h, cells were fixed in 4% formaldehyde (Thermo Scientific Pierce #PI-28906) for 20min on ice, permeabilized with PBS-T (PBS (UCSF Cell Culture Facility) + 0.3% Tween-20 (Sigma-Aldrich #P1379)), blocked with normal goat serum (Abcam, #ab7481) for 1h, incubated with anti-H3S10p for 16h at 4oC and with secondary antibody for 3h at room temperature, and stained with Hoechst 33342 (Molecular Probes #H3570, 5μg/ml) for 10min. 3 PBS-T washes were performed between each step of the protocol, with a final PBS wash. Cells were imaged on a Nikon Ti inverted scope with arc-lamp illumination. Hoechst 33342 was detected using a 350/50nm excitation filter and a 460/50nm emission filter and H3S10p detected using a 470/40nm excitation filter and 525/50nm emission filter (Semrock, Rochester, NY). Cell nuclei were segmented and mitotic fraction was quantified using a custom python script available on github (https://github.com/jpfon/cAMP)

Quantification of acinar area

MDCKI acini were prepared as described in (Elia and Lippincott-Schwart 2010). Over 11 days, acini were exposed to no, low (Duty Cycle = 1.7%) or high (Duty Cycle = 33%) blue light (2mW/cm^2) doses, for 1h of every 48h. Media was replenished at the same rate. Acini were

630 imaged on a Nikon Ti inverted scope using brightfield. Acinar area was quantified using ImageJ
631 (NIH).

632

633 *Imaging of PKAc and quantification of nuclear enrichment*

634 1x10^5 cells were seeded in wells of 8-well slides (Ibidi # 80826) in MEM without phenol red
635 (Gibco # 51200038) supplemented with 0.5% Fetal Calf Serum (VWR #89510-184). After 16h,
636 cells were treated with small molecules or vehicle (DMSO, SIGMA life science #D2650) for 1h.
637 Cells were then exposed to no light or blue light (2mW/cm^2) with different duty cycles for 20min
638 to. Cells were immediately fixed in 4% formaldehyde (Thermo Scientific Pierce #PI-28906) and
639 stained with Hoechst 33342 (5μg/ml). Cells were imaged on a Zeiss microscope equipped with
640 a Yokagawa CSUX1-A1N-E confocal spinning disk. Images were collected with a 40 x 1.1 NA
641 water immersion objective and Photometrics Evolve 512 EMCCD camera. Hoechst 33342 and
642 PRKACA::mRuby2 were detected using the following excitation lines and emission filters:
643 excitation at 405nm, collection between 425 and 475nm for Hoechst 3342; excitation at 561nm,
644 collection between 590 and 650nm for PRKACA::mRuby2. Segmentation of nuclei and
645 quantification of PRKACA Nuclear to Cytoplasmic ratio were performed using a custom python
646 script available on Github (https://github.com/jpfon/cAMP).

647

648 *Data availability*

649 Raw data in this study is available at the UCSF repository (https://doi.org/10.7272/Q6ST7N00).

650

651 *Statistical analysis*

Differences in mitotic fraction were calculated by Fischer's exact test, in acini area by the Kolmogorov-Smirnov test, in PRKACA nuclear enrichment by one-way ANOVA with Tukey-HSD post-tests, and in the effects of Rolipram on PKA activity with a two-way ANOVA. All tests were implemented with Python scripts available on Github (https://github.com/jpfon/cAMP)

Computational model

The computational model representing the cAMP-PKA signaling network is described in the Supplementary Information. Model simulations and optimization were performed with Python scripts available on Github (https://github.com/jpfon/cAMP)

Acknowledgements

We thank Leonardo Morsut for the blue light LEDs and controllers; the El-Samad lab members, Marisa Rosa, Jeremy Chang, Zara Weinberg and Jeremy Reiter for critical feedback on the manuscript. This work was supported by the National Science Foundation through grant NSF-MCB 1715108 to HES

Figure Legends

Figure 1.

PKA and ERK have a biphasic response to cAMP

(A) Simplified schematic of cAMP-PKA pathway, illustrating the canonical relationship between cAMP and PKA as well as the activating effect of cAMP on ERK and a known inhibitory link from PKA onto ERK. bPAC-generated cAMP activates PKA. Active PKA phosphorylates its targets and

674 inhibits ERK. Quantified variables present in Figure 1 are shown in red **(B)** Intracellular cAMP
675 concentration of MDCKI and MDCKI + bPAC in dark (Control) and after 20min of constant blue
676 light exposure (Light). Box plots indicate distribution quartiles and whiskers indicate the rest of
677 distribution. Data points from biological and technical replicates used to generate distributions are
678 plotted. **(C)** Intracellular cAMP concentration of MDCKI + bPAC cells at 20 minutes of light
679 treatment with different duty cycles for period equal to 30s (%, T=30s). Data points are shown in
680 log scale, together with mean and 95% confidence interval of fit of a hyperbolic equation ($cAMP =$
681 $\frac{a \times DutyCycle}{b + DutyCycle} + c$) to data. **(D)** Immunoblots of PKA and ERK activity (measured with Phospho-PKA
682 substrate and Phospho-ERK1/2 antibodies) of parental MDCKI and MDCKI + bPAC cells after
683 20min of light treatment with different duty cycles. Alpha-Tubulin (Tub.) was used for
684 normalization. **(E)** Quantification of PKA activity and **(F)** ERK activity from panel (C) for different
685 cAMP concentrations in MDCKI + bPAC cells. Insets show relationship of signaling activity to duty
686 cycle for both MDCKI and MDCKI + bPAC cells. Error bars represent 95% confidence intervals
687 of mean for at least 3 replicates.

688

689 Figure 2.

690 **PKA inhibition is independent of PDE activity and association of PKA subunits.**

691 **(A)** Quantification of PKA activity (measured with Phospho-PKA substrate antibody) of MDCKI +
692 bPAC cells treated with DMSO or PDE inhibitor (Rolipram (10μM)) and subsequently exposed to
693 20min of blue light with different duty cycles. * identifies p-value <0.05 in a two-way ANOVA test
694 for the interaction between treatment and duty cycle. Errorr bars show 95% confidence intervals
695 of mean for at least 3 replicates. **(B)** Images of fixed MDCKI and MDCKI + bPAC cells, expressing
696 PRKACA fused to mRuby2 and stained with Hoechst 3342. Scale bar represents 10μm. Parental
697 MDCKI and MDCKI + bPAC were treated with adenylyl cyclase agonist Forskolin (50μM) or with

PKA inhibitor H89(10μM) or subjected to 2h of low (duty cycle = 1.7%) and high (duty cycle = 33.3%) cAMP doses. Quantification of PRKACA enrichment in nuclei (Nuclear PRKACA / Cytoplasmic PRKACA) is shown below. Box plot height indicates inter-quartile deviation. Median, minimum and maximum values of distribution are shown. * and ** identify p-values <0.05 and <0.01 in a Tukey-HSD multiple comparison after ANOVA. Quantification of each condition and genotype was performed in at least 20 cells.

Figure 3.

MAPK activation inhibits PKA activity at high cAMP doses

(A) Schematic of the interactions between cAMP, PKA and MAPK. These interactions are represented in the computational model. bPAC-generated cAMP activates PKA, ERK and p38. Active PKA phosphorylates its targets and inhibits ERK. P38 and ERK inhibit PKA activity. SB202190 inhibits p38 activity and U0126 inhibits ERK activation. Experimentally measured variables are shown in red. **(B)** Immunoblots of p38 activity (measured with Phospho-p38 antibody) of MDCKI and MDCKI + bPAC cells after 20min of light treatment with different duty cycles. Alpha-Tubulin (Tub.) was used for normalization. **(C)** Quantification of p38 activity from (B) for different cAMP concentrations in MDCKI + bPAC cells. Inset shows relationship between p38 activity and duty cycle in MDCKI and MDCKI + bPAC cells. **(D)** Quantification of PKA activity (measured with Phospho-PKA substrate antibody) of MDCKI + bPAC cells treated with DMSO or MEK inhibitor (U0126 (10μM)) or p38 inhibitor (SB202190 (10μM)) and subsequently exposed to 20min of blue light with different duty cycles. Quantification of westerns in (C) and (D) was performed in at least 3 replicates. Error bars show 95% confidence intervals of mean. **(E)** Ratio of PKA activity in MDCKI+ bPAC cells treated with SB203580 and U0126 to those treated with DMSO when exposed to light inputs with different duty cycles for 20min. **(F)** Color scheme in (F)

722 through (L) is the same as in (D) and (E). Filled circles and solid line represent experimental data,
723 while dashed line represents simulations. Model simulation results of PKA activity of of MDCKI +
724 bPAC cells treated with DMSO or MEK inhibitor (U0126 (10μM)) or p38 inhibitor (SB202190
725 (10μM)) and subsequently exposed to 20min of blue light with different duty cycles. **(G)** Model
726 simulation results of ratio of PKA activity in MDCKI+ bPAC cells treated with SB203580 and
727 U0126 to those treated with DMSO when exposed to light inputs with different duty cycles for
728 20min. **(H)** Model simulation results of ERK activity of MDCKI+bPAC cells treated with DMSO,
729 SB202190 and U0126 and exposed to blue light with different duty cycles. **(I)** Model simulation
730 results of p38 activity of MDCKI+bPAC cells treated with DMSO, SB202190 and U0126 and
731 exposed to blue light with different duty cycles. **(J)** Magnitude of PKA inhibition of ERK predicted
732 by computational model (PKA -| ERK) as a function of duty cycle for MDCKI+ bPAC cells in the
733 presence of DMSO, U0126 or SB202190. PKA -| ERK was defined as $ERKa \times \frac{\beta I_{PKA}^{nI_{PKA}} \times PKAa^{nI_{PKA}}}{KmI_{PKA}^{nI_{PKA}} + PKAa^{nI_{PKA}}}$
734 (see Supplementary Information for more detail). **(K)** Magnitude of ERK inhibition of PKA
735 predicted by computational model (ERK -| PKA) as a function of duty cycle for MDCKI+ bPAC
736 cells in the presence of DMSO, U0126 or SB202190. ERK -| PKA was defined
737 as $PKAa \times \frac{\beta I_{ERK}^{nI_{ERK}} \times ERKa^{nI_{ERK}}}{KmI_{ERK}^{nI_{ERK}} + ERKa^{nI_{ERK}}}$ (see Supplementary Information for more detail). **(L)** Magnitude of
738 p38 inhibition of PKA predicted by computation model (p38 -| PKA) as a function of duty cycle for
739 MDCKI+ bPAC cells in the presence of DMSO, U0126 or SB202190. P38 -| PKA was defined
740 as $PKAa \times \frac{\beta I_{p38}^{nI_{p38}} \times p38a^{nI_{p38}}}{KmI_{p38}^{nI_{p38}} + p38a^{nI_{p38}}}$ (see Supplementary Information for more detail).

741

742 Figure 4.

743 **Different cAMP doses produce different transcriptional responses**

744 **(A)** Normalized expression level of differentially expressed genes (n = 3421) of MDCKI + bPAC
745 cells after 2h of low and high cAMP doses (Duty Cycles of 1.7% and 33%, respectively).
746 Hierarchical clustering of correlated gene expression identifies 8 clusters. **(B)** Mean expression
747 of genes included in the clusters identified in (A) for different cAMP inputs and total number of
748 genes included in each cluster. **(C)** Scatter plot of all differentially expressed genes with their
749 response in low cAMP dose versus high cAMP dose. Clusters 1 and 2, whose genes activity
750 correlate with ERK1/2 activity are identified with color (light blue, Cluster 1; dark blue, Cluster 2).
751 Selected genes for 3 GO terms enriched in Clusters 1 and 2 are identified: desmosome
752 organization (GO:0002934, black), stress activated MAPK cascade (GO:0051403, green) and
753 positive regulation of respiratory burst (GO:0060267, blue). **(D)** Scatter plot of all differentially
754 expressed genes with their response in low cAMP dose versus high cAMP dose. Clusters 3 and
755 4, whose genes activity correlate with PKA activity are identified with color (light green, Cluster 3;
756 dark green, Cluster 3). Selected genes for 4 GO terms enriched in Clusters 3 and 4 are identified:
757 chromatin remodeling (GO:0006338, black), positive regulation of branching involved in ureteric
758 bud morphogenesis and mesonephros development (GO:0090190 and GO:0001823, green) and
759 negative regulation of cell population proliferation (GO:0008285, blue).

760

761 Figure 5.

762 **cAMP dose differentially regulates AKT signaling, proliferation and acini growth**

763 **(A)** Proliferation rate of cells through measurement of phosphorylation of histone H3S10. MDCKI
764 and MDCKI + bPAC cells were subjected to 2h of low (duty cycle = 1.7%, green) and high (duty
765 cycle = 33.3%, pink) cAMP doses. After 14h, phosphorylation of histone H3S10 was quantified
766 by immunofluorescence. Images show cell nuclei stained with Hoechst 3342 (magenta) and
767 histone H3S10 phosphorylation (green). Mitotic fractions, normalized to cells not subjected to

768 cAMP are show at the bottom. * identifies a p-value <0.01 in Fisher's exact test. **(B)** Images of
769 acini structures. MDCKI and MDCKI + bPAC cells, grown in collagen I gel, were subjected to 2h
770 of low (duty cycle = 1.7%, green) and high (duty cycle = 33.3%, pink) cAMP doses every 48h for
771 11 days. Acini were imaged at their center and the area quantified. Data points used to generate
772 distributions are plotted below. * identifies a p-value <0.05 in Kolmogorov-Smirnov test.

773

774 Supplementary Figure 1.

775 **Time course of CREB, PKA and ERK1/2 activity of MDCKI and MDCKI + bPAC cells treated**
776 **with two cAMP doses**

777 **(A)** Immunoblots of PKA, CREB and ERK activity (measured with Phospho-PKA substrate,
778 Phospho-CREB and Phospho-ERK antibodies) of MDCKI and MDCKI + bPAC cells treated for 0,
779 5, 10, 20, 30, 60 and 90 minutes with low and high cAMP doses (Duty Cycle = 1.7% and 33%,
780 respectively). **(B)** Quantification of immunoblots show in (A). Quantification was performed in at
781 least 3 replicates.

782

783 Supplementary Figure 2

784 **ERK activity of MDCKI + bPAC cells treated with light and PKA inhibitor H89**

785 **(A)** Immunoblots of ERK activity (measured with Phospho-ERK antibody) of MDCKI+ cells treated
786 with DMSO or PKA inhibitor (H89 (10μM)) and subsequently exposed to 20min of blue light with
787 different duty cycles. **(B)** Quantification of immunoblot shown in (A)

788

789 Supplementary Figure 3

PKA activity of MDCKI + bPAC cells treated with light and PDE inhibitor Rolipram

Immunoblots of PKA activity (measured with Phospho-PKA substrate antibody) of MDCKI + bPAC cells treated with DMSO or PDE inhibitors (Rolipram (10μM)) and subsequently exposed to 20min of blue light with different duty cycles.

Supplementary Figure 4

PKA activity of MDCKI + bPAC cells treated with light and different MAPKs inhibitors

Immunoblots of PKA activity (measured with Phospho-PKA substrate antibody) of MDCKI + bPAC cells treated with DMSO, MEK inhibitor (U0126 (10 μM)) or p38 inhibitor (SB203580 (10 μM)) and subsequently exposed to 20min of blue light with different duty cycles.

Supplementary Figure 5

Distributions of cAMP-PKA model parameters

(A) Distributions (diagonal) and pair-wise joint distributions of parameter values in the cAMP-PKA computational model that were able to describe PKA, ERK and p38 activity in the presence of DMSO, and PKA in the presence of U0126 and SB202190. **(B)** Distributions of Km_{PKA} (blue), Km_{ERK} (green) and Km_{p38} (red). Most fitted Km_{PKA} parameters are smaller than Km_{ERK} and Km_{p38}. **(C)** Relationship between Km_{PKA} and n_{PKA}. For large Km_{PKA}, n_{PKA} is always small. **(D)** Relationship between Km_{PKA}, and the ratio of n_{PKA} to n_{ERK} (blue) or to n_{p38} (red). n_{PKA} is much smaller than n_{ERK} and n_{p38} for large Km_{PKA}. **(E)** Distributions of nI_{PKA} (blue), nI_{ERK} (green) and nI_{p38} (red). Fitted nI_{ERK} parameters are always large. Detailed description of model and simulations in Supplementary Information.

Supplementary Figure 6

Effect of bPAC expression in MDCKI transcriptome

(A) Volcano plot identifying genes that are repressed (magenta) or overexpressed (green) upon expression of bPAC in MDCKI cells. **(B)** Normalized expression level of genes regulated by bPAC presence (n = 371) in MDCKI + bPAC cells after 2h of low and high cAMP doses (Duty Cycles of 1.7% and 33%, respectively). Repression or upregulation upon bPAC expression does not inform of behavior upon additional cAMP input. Membership in clusters identified in Figure 4 is shown on the left (92 genes) as well as positive or negative effect of bPAC expression.

Supplementary Figure 7.

Validation of RNAseq results with qPCR

(A) RNA sequencing counts and **(B)** qPCR quantification for NR4A2, PAX8, PER1 and GATA3 genes in MDCKI and MDCKI + bPAC cells exposed to blue light for 2h with different duty cycles for period (T) equal to 30s (0%, 1.7% and 33 or 100%). qPCR was performed from at least 3 independent RNA isolations.

Supplementary Figure 8.

Transcription factor and Kinase Perturbation associated with differentially expressed genes

(A) Top twenty transcription factors from ChEA 2016 database in Enrichr tool whose binding is enriched in the promotors of the genes included in the clusters identified in Figure 4. **(B)** Top twenty transcription factor perturbations from Transcription Factor Perturbation database in

Enrichr tool whose transcriptome correlates to the genes included in the clusters identified in Figure 4. **(C)** Top twenty kinase perturbations from Kinase Perturbation - GEO down database in Enrichr tool whose downregulated genes correlate to the genes included in the clusters identified in Figure 4. **(D)** Top twenty kinase perturbations from Kinase Perturbation - GEO up database in Enrichr tool whose upregulated genes correlate to the genes included in the clusters identified in Figure 4.

Supplementary Figure 9.

GO terms enriched in clusters of differentially expressed genes

(A) REVIGO plot of GO terms enriched in clusters 1 and 2, **(B)** clusters 3 and 4, **(C)** clusters 4 and 5 and **(D)** clusters 7 and 8. Clusters were identified in Figure 4.

Supplementary Figure 10.

AKT activity in MDCKI and MDCKI + bPAC cells

(A) Immunoblots of AKT activity (measured with Phospho-AKT antibody) of MDCKI + bPAC cells after 20min of light treatment with different duty cycles. Alpha-Tubulin (Tub.) was used for normalization. **(B)** Quantification of immunoblots in (A)

Supplementary Table 1. List of differential expressed genes and their adjusted p-value, log fold change and cluster identity. Related to Figure 4.

Supplementary Table 2. List of primers used for qPCR. Related to Supplementary Figure 7.

Supplementary Information. Description of computational model and parameters used in simulations. Related to Figure 3.

References

1. Canaves JM, Taylor SS. Classification and phylogenetic analysis of the cAMP-dependent protein kinase regulatory subunit family. J Mol Evol. 2002 January 01;54(1):17-29.

2. Beavo JA, Brunton LL. Cyclic nucleotide research - still expanding after half a century. Nature Reviews Molecular Cell Biology. 2002 Sep;3(9):710-8.

3. Sassone-Corsi P. The Cyclic AMP Pathway. Cold Spring Harbor perspectives in biology. 2012 Dec 1,;4(12):a011148.

4. Walsh DA, Perkins JP, Krebs EG. Communications. Communications. 1968 07/10/;243(13):3763-5.

5. Skalhegg BS, Tasken K. Specificity in the cAMP/PKA signaling pathway. Differential expression,regulation, and subcellular localization of subunits of PKA. Front Biosci. 2000 Aug 01,;5:678.

6. Shabb JB. Physiological Substrates of cAMP-Dependent Protein Kinase. Chem Rev. 2001 August 1,;101(8):2381-412.

7. Isobe K, Jung HJ, Yang C, Claxton J, Sandoval P, Burg MB, et al. Systems-level identification of PKA-dependent signaling in epithelial cells. PNAS. 2017 -10-17 00:00:00;114(42):E8884.

8. Taylor SS, Zhang P, Steichen JM, Keshwani MM, Kornev AP. PKA: Lessons learned after twenty years. Biochimica et Biophysica Acta (BBA) - Proteins and Proteomics. 2013 July 1,;1834(7):1271-8.

9. Ma N, Abel T, Hernandez PJ. Exchange protein activated by cAMP enhances long-term memory formation independent of protein kinase A. Learning & memory (Cold Spring Harbor, N.Y.). 2009 Jun;16(6):367-70.

10. Efetova M, Petereit L, Rosiewicz K, Overend G, Haussig F, Hovemann BT, et al. Separate roles of PKA and EPAC in renal function unraveled by the optogenetic control of cAMP levels in vivo. J Cell Sci. 2013 February 01;126(Pt 3):778-88.

11. Ruat M, Traiffort E, Leurs R, Tardivel-Lacombe J, Diaz J, Arrang JM, et al. Molecular cloning, characterization, and localization of a high-affinity serotonin receptor (5-HT7) activating cAMP formation. PNAS. 1993 -09-15 00:00:00;90(18):8547-51.

12. Vaibhav P. Pai, Nelson D. Horseman. Biphasic Regulation of Mammary Epithelial Resistance by Serotonin through Activation of Multiple Pathways. Journal of Biological Chemistry. 2008 Nov 7,;283(45):30901-10.

13. Carrozzino F, Feraille E, Montesano R, Pugnale P. Inhibition of basal p38 or JNK activity enhances epithelial barrier function through differential modulation of claudin expression. The American Journal of Physiology. 2009 Sep 1,;297(3):C775.

14. Stierl M, Stumpf P, Udwari D, Gueta R, Hagedorn R, Losi A, et al. Light modulation of cellular cAMP by a small bacterial photoactivated adenylyl cyclase, bPAC, of the soil bacterium Beggiatoa. The Journal of biological chemistry. 2011 Jan 14,;286(2):1181.

15. Jansen V, Alvarez L, Balbach M, Strunker T, Hegemann P, Kaupp UB, et al. Controlling fertilization and cAMP signaling in sperm by optogenetics. Elife. 2015 January 20;4:10.7554/eLife.05161.

16. Stewart-Ornstein J, Chen S, Bhatnagar R, Weissman JS, El-Samad H. Model-guided optogenetic study of PKA signaling in budding yeast. Molecular biology of the cell. 2017 Jan 1,;28(1):221-7.

17. Dukes JD, Whitley P, Chalmers AD. The MDCK variety pack: choosing the right strain. BMC cell biology. 2011 Oct 7,;12(1):43.

18. Mangoo-Karim R, Uchic M, Lechene C, Grantham JJ. Renal epithelial cyst formation and enlargement in vitro: dependence on cAMP. PNAS. 1989 -08-01 00:00:00;86(15):6007-11.

19. Yamaguchi T, Pelling JC, Ramaswamy NT, Eppler JW, Wallace DP, Nagao S, et al. cAMP stimulates the in vitro proliferation of renal cyst epithelial cells by activating the extracellular signal-regulated kinase pathway. Kidney International. 2000 Apr;57(4):1460-71.

20. Azeloglu EU, Hardy SV, Eungdamrong NJ, Chen Y, Jayaraman G, Chuang PY, et al. Interconnected Network Motifs Control Podocyte Morphology and Kidney Function. Sci Signal. 2014 -02-04 00:00:00;7(311):ra12.

21. Deb DK, Bao R, Li YC. Critical role of the cAMP-PKA pathway in hyperglycemia-induced epigenetic activation of fibrogenic program in the kidney. FASEB Journal. 2017 May 1,;31(5):2065-75.

22. Stierl M, Stumpf P, Udwari D, Gueta R, Hagedorn R, Losi A, et al. Light modulation of cellular cAMP by a small bacterial photoactivated adenylyl cyclase, bPAC, of the soil bacterium Beggiatoa. J Biol Chem. 2011 January 14;286(2):1181-8.

23. Nedvetsky PI, Kwon S, Debnath J, Mostov KE. Cyclic AMP regulates formation of mammary epithelial acini in vitro. Molecular biology of the cell. 2012 Aug;23(15):2973-81.

24. Stork PJS, Schmitt JM. Crosstalk between cAMP and MAP kinase signaling in the regulation of cell proliferation. Trends in Cell Biology. 2002;12(6):258-66.

923 25. Murray AJ. Pharmacological PKA Inhibition: All May Not Be What It Seems. Sci Signal. 2008
924 -06-03 00:00:00;1(22):re4.

925 26. C Sette, M Conti. Phosphorylation and activation of a cAMP-specific phosphodiesterase by
926 the cAMP-dependent protein kinase. Involvement of serine 54 in the enzyme activation. The
927 Journal of biological chemistry. 1996 Jul 12,;271(28):16526-34.

928 27. Alexandre Gidon, Mohammad M Al-bataineh, Frederic G Jean-alphonse, Hilary P
929 Stevenson, Tomoyuki Watanabe, Claire Louet, et al. Endosomal GPCR signaling turned off by
930 negative feedback actions of PKA and v-ATPase. Nature Chemical Biology. 2014 Sep
931 1,;10(9):707-9.

932 28. Gong K, Li Z, Xu M, Du J, Lv Z, Zhang Y. A Novel Protein Kinase A-independent, β-Arrestin-
933 1-dependent Signaling Pathway for p38 Mitogen-activated Protein Kinase Activation by β2-
934 Adrenergic Receptors. Journal of Biological Chemistry. 2008 Oct 24,;283(43):29028-36.

935 29. Love MI, Huber W, Anders S. Moderated estimation of fold change and dispersion for RNA-
936 seq data with DESeq2. Genome biology. 2014;15(12):550.

937 30. Huang DW, Sherman BT, Tan Q, Kir J, Liu D, Bryant D, et al. DAVID Bioinformatics
938 Resources: expanded annotation database and novel algorithms to better extract biology from
939 large gene lists. Nucleic Acids Res. 2007 /07/01;35(suppl_2):W175.

940 31. Kuleshov MV, Jones MR, Rouillard AD, Fernandez NF, Duan Q, Wang Z, et al. Enrichr: a
941 comprehensive gene set enrichment analysis web server 2016 update. Nucleic Acids Res. 2016
942 /07/08;44(W1):W97.

943 32. Liaohan Ouyang, Kirsten K. Jacob, Frederick M. Stanley. GABP Mediates Insulin-increased
944 Prolactin Gene Transcription. Journal of Biological Chemistry. 1996 May 3,;271(18):10425-8.

945 33. Ramesh Narayanan, Veronica A. Tovar Sepulveda, Miriam Falzon, Nancy L. Weigel. The
946 Functional Consequences of Cross-talk between the Vitamin D Receptor and ERK Signaling
947 Pathways Are Cell-specific. Journal of Biological Chemistry. 2004 Nov 5,;279(45):47298-310.

948 34. Gonzalez GA, Montminy MR. Cyclic AMP stimulates somatostatin gene transcription by
949 phosphorylation of CREB at serine 133. Cell. 1989;59(4):675-80.

950 35. TEXTOR B, SATOR-SCHMITT M, RICHTER KH, ANGEL P, SCHORPP-KISTNER M. c-Jun
951 and JunB Are Essential for Hypoglycemia-Mediated VEGF Induction. Annals of the New York
952 Academy of Sciences. 2006 Dec;1091(1):310-8.

953 36. Iglesias-Bartolome R, Torres D, Marone R, Feng X, Martin D, Simaan M, et al. Inactivation
954 of a Gα s –PKA tumour suppressor pathway in skin stem cells initiates basal-cell
955 carcinogenesis. Nature Cell Biology. 2015 Jun;17(6):793-803.

956 37. Andrew DJ, Ewald AJ. Morphogenesis of epithelial tubes: Insights into tube formation,
957 elongation, and elaboration. Developmental Biology. 2010;341(1):34-55.

958 38. Huebner RJ, Neumann NM, Ewald AJ. Mammary epithelial tubes elongate through MAPK-
959 dependent coordination of cell migration. Development (Cambridge, England). 2016 Mar
960 15,;143(6):983-93.

961 39. Carolyn E. Fisher, Lydia Michael, Mark W. Barnett, Jamie A. Davies. Erk MAP kinase
962 regulates branching morphogenesis in the developing mouse kidney. Development. 2001 Nov
963 1,;128(21):4329-38.

964 40. Valentich JD. Morphological similarities between the dog kidney cell line MDCK and the
965 mammalian cortical collecting tube. Annals of the New York Academy of Sciences. 1981;372(1
966 Hormonal Regu):384-405.

967 41. Valentich JD, Tchao R, Leighton J. Hemicyst formation stimulated by cyclic AMP in dog
968 kidney cell line MDCK. Journal of cellular physiology. 1979 Aug;100(2):291-304.

969 42. Yong Wan, Xin-Yun Huang. Analysis of the Gs/Mitogen-activated Protein Kinase Pathway in
970 Mutant S49 Cells. Journal of Biological Chemistry. 1998 Jun 5,;273(23):14533-7.

971 43. K. A. DeFea, J. Zalevsky, M. S. Thoma, O. Déry, R. D. Mullins, N. W. Bunnett. β-Arrestin-
972 Dependent Endocytosis of Proteinase-Activated Receptor 2 Is Required for Intracellular
973 Targeting of Activated ERK1/2. The Journal of Cell Biology. 2000 Mar 20,;148(6):1267-81.

974 44. Tohgo A, Pierce KL, Choy EW, Lefkowitz RJ, Luttrell LM. β-Arrestin Scaffolding of the ERK
975 Cascade Enhances Cytosolic ERK Activity but Inhibits ERK-mediated Transcription following
976 Angiotensin AT1a Receptor Stimulation. The Journal of biological chemistry. 2002 Mar
977 15,;277(11):9429-36.

978 45. Stefan E, Malleshaiah MK, Breton B, Ear PH, Bachmann V, Beyermann M, et al. PKA
979 regulatory subunits mediate synergy among conserved G-protein-coupled receptor cascades.
980 Nature Communications. 2011 -12-20;2:598.

981 46. Hart Y, Alon U. The Utility of Paradoxical Components in Biological Circuits. Molecular Cell.
982 2013 Jan 24,;49(2):213-21.

983 47. Kim D, Kwon Y, Cho K. The biphasic behavior of incoherent feed-forward loops in
984 biomolecular regulatory networks. BioEssays : news and reviews in molecular, cellular and
985 developmental biology. 2008 Nov;30(11-12):1204-11.

986 48. Dekel E, Bren A, Alon U, Kaplan S. The incoherent feed-forward loop can generate non-
987 monotonic input functions for genes. Molecular Systems Biology. 2008 Jul 15,;4(1):n/a.

988 49. Torres VE. Therapies to Slow Polycystic Kidney Disease. Nephron Experimental
989 Nephrology. 2004 Sep;98(1):e7.

990 50. Supek F, Bošnjak M, Škunca N, Šmuc T. REVIGO Summarizes and Visualizes Long Lists of
991 Gene Ontology Terms. PLOS ONE. 2011 Jul 18,;6(7):e21800.

992

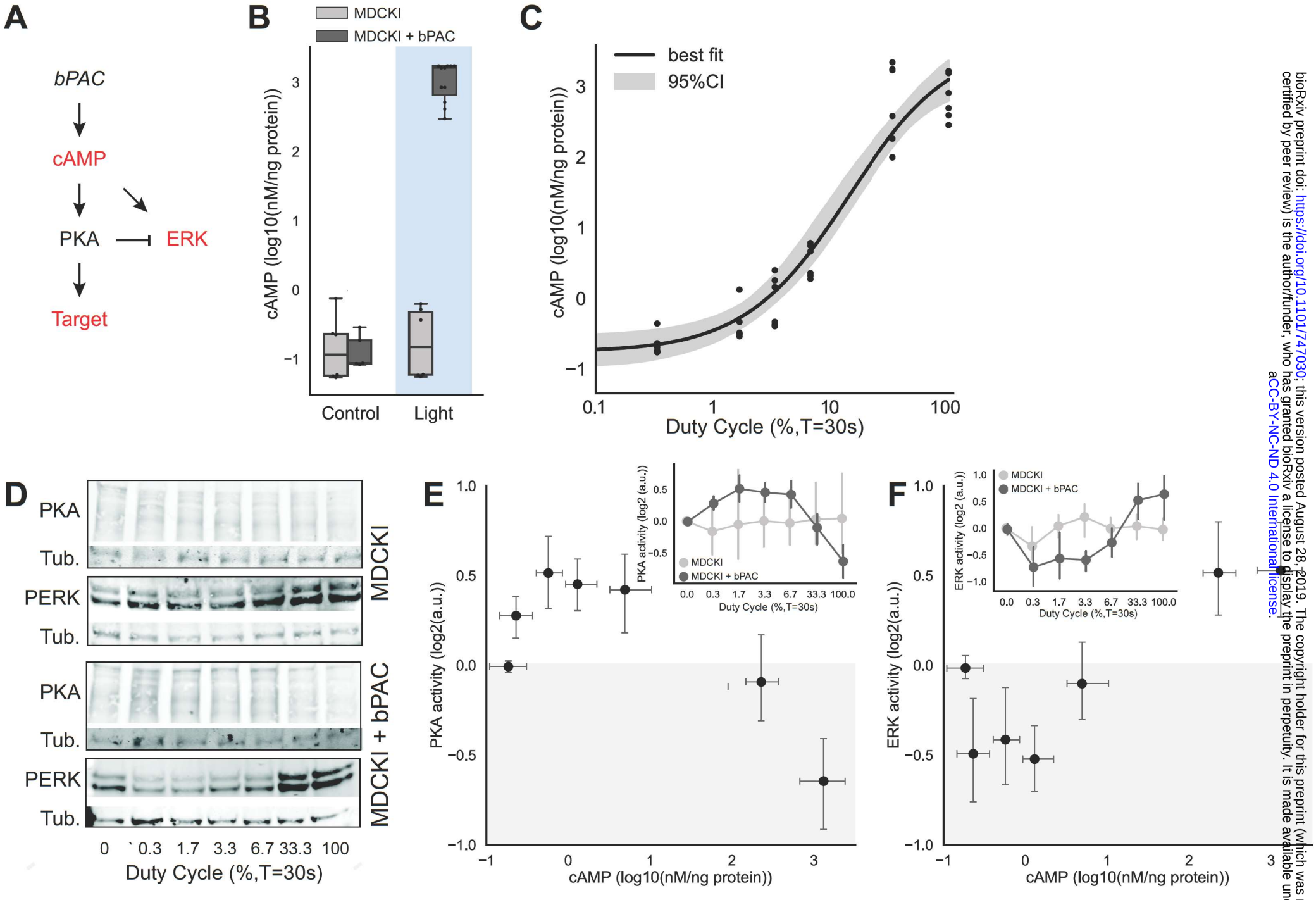

Figure 1

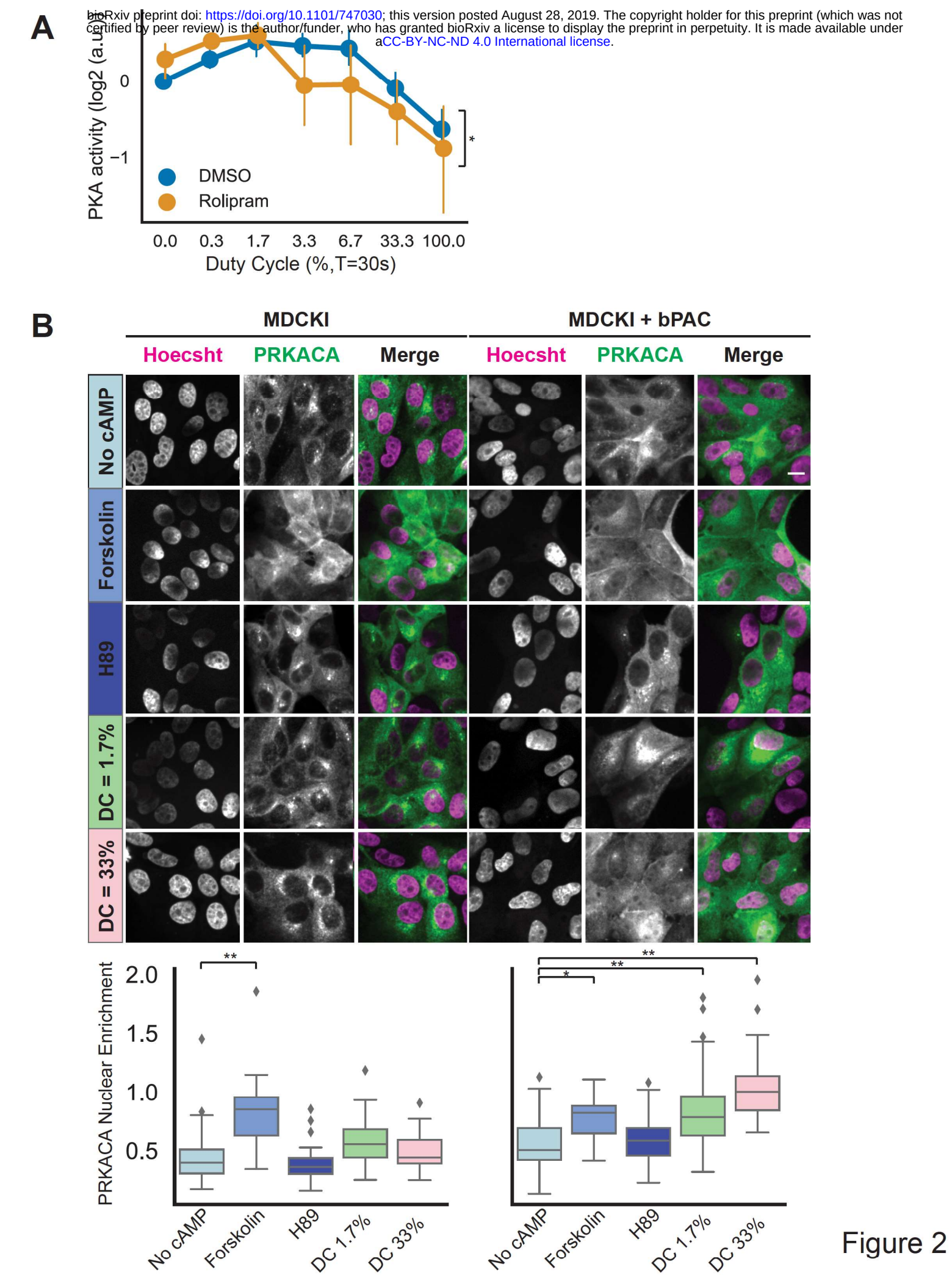

Figure 2

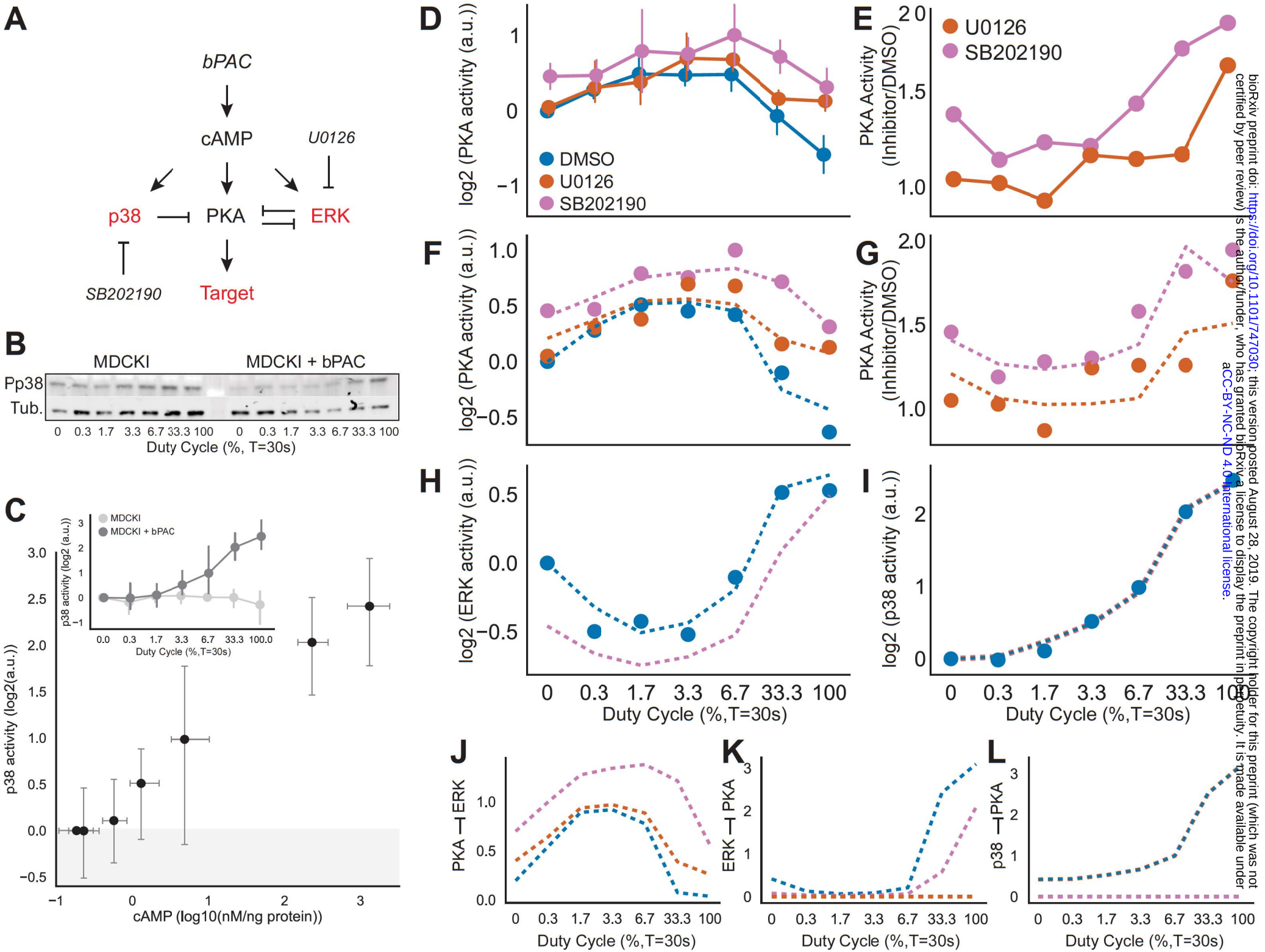

Figure 3

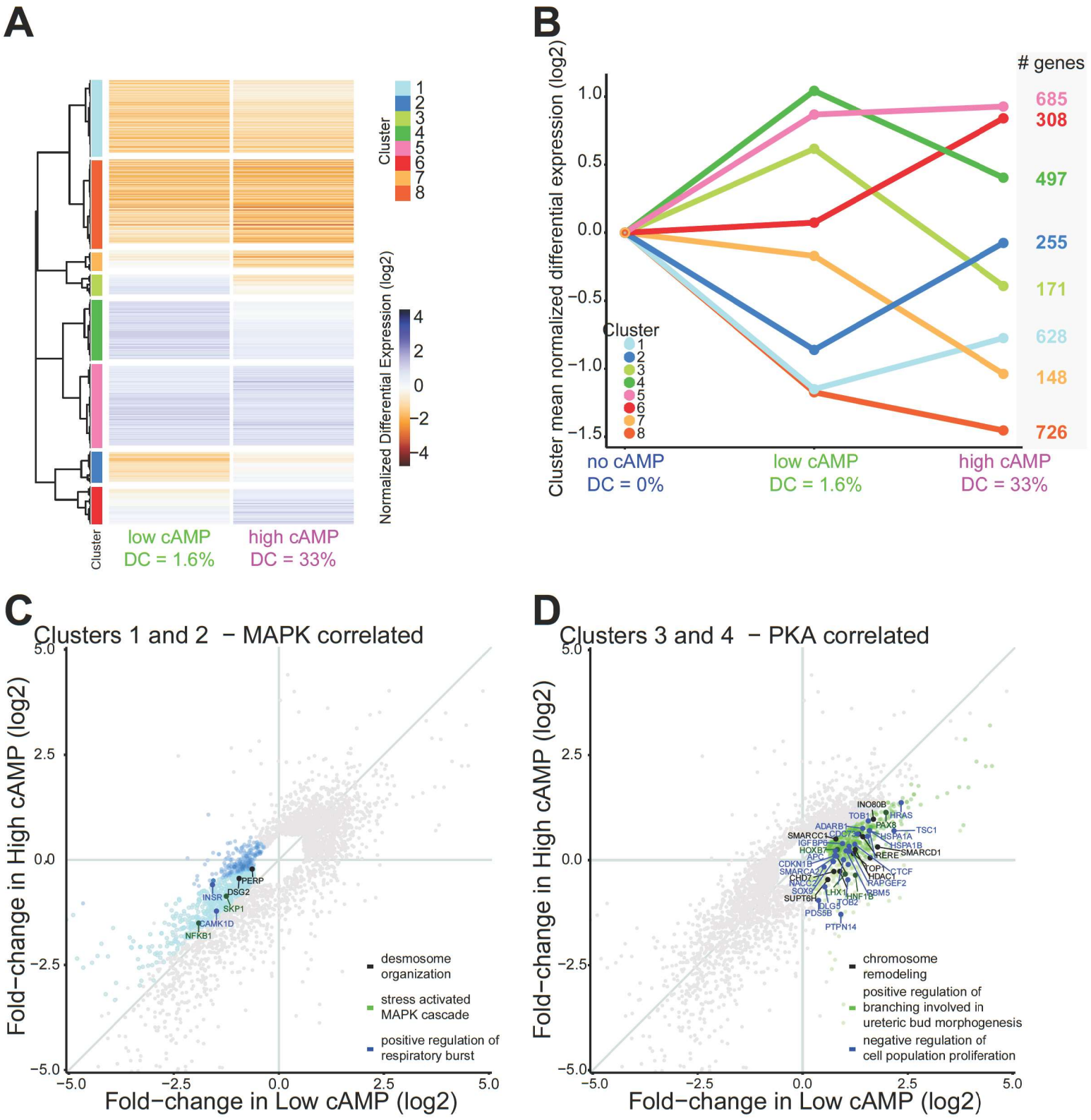

Figure 4

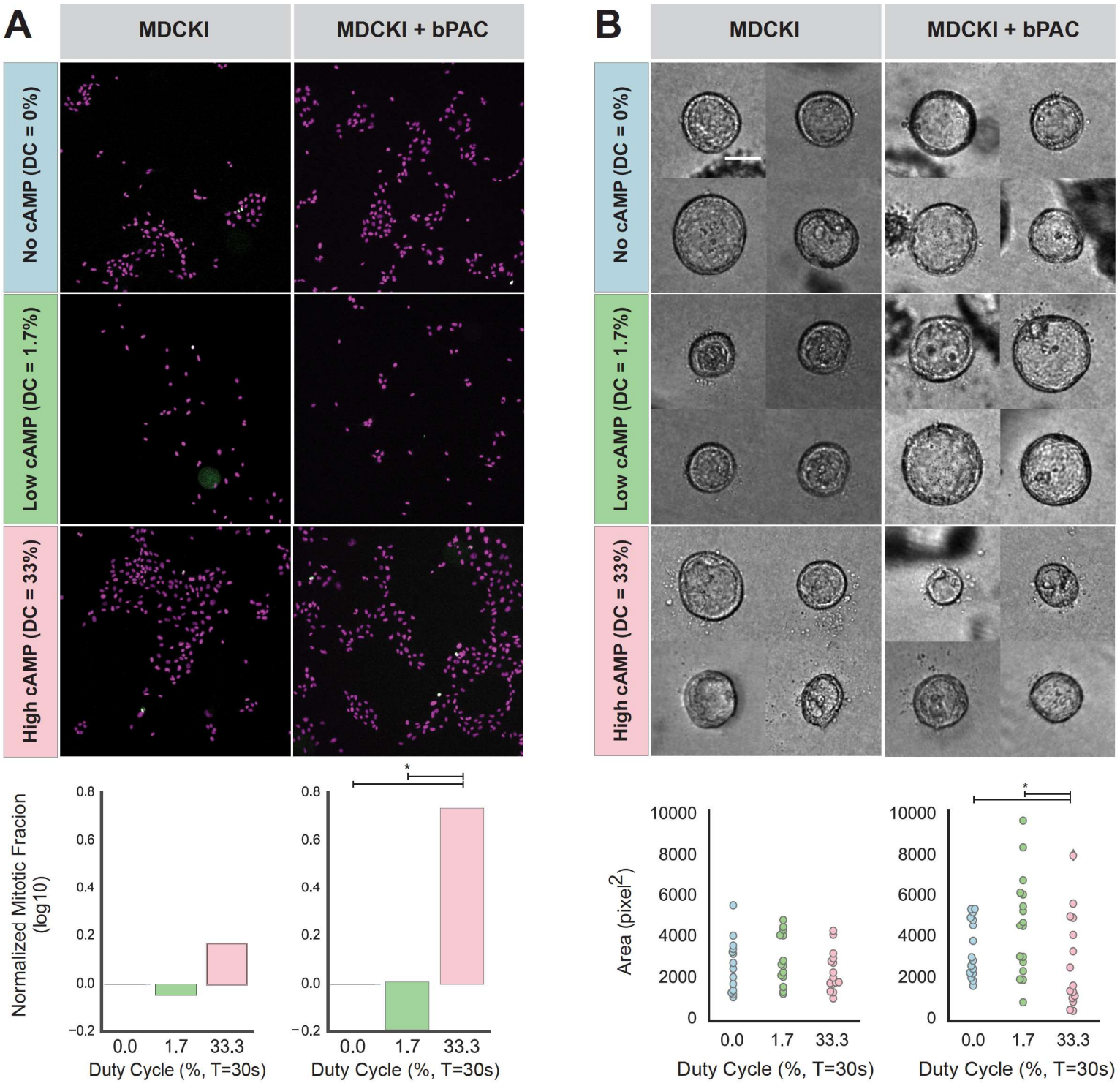

Figure 5